



Theoretical and experimental analysis of the oxidation of CO on Pt catalysts supported on modified TiO₂(101)



Cecilia I.N. Morgade^{a,b}, Charito I. Vignatti^c, M. Sol Avila^c, Gabriela F. Cabeza^{a,*}

^a Grupo de Materiales y Sistemas Catalíticos, Departamento de Física (IFISUR) Universidad Nacional del Sur, Av. Alem 1253, Bahía Blanca B8000CP, Argentina

^b Universidad Tecnológica Nacional, 11 de Abril 461, Bahía Blanca B8000CP, Argentina

^c GICIC (Catalysis Science and Engineering Research Group) – INCAPe (Instituto de Investigaciones en Catálisis y Petroquímica), Santiago del Estero 2654, Santa Fe, Argentina

ARTICLE INFO

Article history:

Received 13 February 2015

Received in revised form 16 June 2015

Accepted 17 June 2015

Available online 23 June 2015

ABSTRACT

The dynamics of the CO adsorption on Pt nanoparticles deposited on TiO₂(101) (pure, N-doped and/or reduced) have been investigated using UV-visible diffuse reflectance spectroscopy, diffuse reflectance infrared Fourier transform spectroscopy and density functional theory. The results point to that N-doping and oxygen vacancies in the Pt/N-TiO₂ system should favor catalytic reactions in which CO conversion into CO₂ takes place mediated by support surface O atoms.

© 2015 Elsevier B.V. All rights reserved.

Keywords:

CO oxidation

Pt/N-TiO₂(101)

O vacancies

DFT

DRIFTS

1. Introduction

The metal–oxide interaction plays an important role in heterogeneous catalysis. Oxides are commonly used as support and thus help to stabilize the nanoparticles and disperse active metal on the support, avoiding sintering and deactivation. However, the support does not always remain inactive. Many studies point to the importance of the connection of the three phases (gas, metal and support) but the nature of the relationship between the metal and the support is not yet understood [1]. Frequently, the strong interaction between them causes drastic changes in the chemisorptive properties of metals. Besides, the work function of noble metals (ranges from 4.5 eV to 6 eV) is generally greater than that of the semiconductor so is expected that electron transfer occurs from the oxide to the metal. This interaction has been motive of study, especially in water gas shift reaction (WGS: CO + H₂O ⇌ CO₂ + H₂).

Several studies have demonstrated that Pt-based catalysts are more active in WGS in comparison with other noble metals (Pd, Au) [2–8]. Moreover, platinum activity is highly dependent on the material support [9]. In particular, CO conversion turnover rate is

about two orders of magnitude higher on Pt/TiO₂ than on Pt/SiO₂ [9]. Kalamaras et al. [10], based on SSITKA-DRIFTS, SSITKA-MS and other transient ¹⁸O-isotope exchange experiments, suggested that the WGS reaction on Pt/TiO₂ is promoted by a redox bifunctional mechanism in which CO adsorbs on Pt, diffuses towards the metal–support interface, and reacts with labile oxygen of the titania to form CO₂ generating oxygen defect sites in the process. In this mechanism, the reduced titania formed is oxidized by H₂O releasing H₂. The authors also proposed that oxygen vacancies on the support contribute to the activation of water. Based on this study, the increase of oxygen vacancies and/or labile oxygen in the support would favor Pt/TiO₂ performance toward water gas shift reaction.

In other systems such as Au/MgO, oxygen vacancy sites were found to play a dominant role in anchoring and activating the metal clusters by (partial) charge-transfer [11]. Studying the influence of the vacancies is crucial because in some chemical reactions, as the WGS, it is believed that the catalytic activity of the support is largely dependent on the density of defects in the exposed surface. The chemical and electronic properties of surfaces to a large extent are controlled by defects. Defects facilitate the adsorption of gases and serve as reactive sites for chemical reactions. Liu et al. [12] have shown that defects are predominantly vacancies of oxygen and Ti⁺³ ions. It has been demonstrated that the surface chemistry of stoichiometric anatase shows marked differences with respect

* Corresponding author. Fax: +54 291 4595142.

E-mail address: gcabeca@uns.edu.ar (G.F. Cabeza).

to the reduced surface as a consequence of the oxygen vacancies. There is experimental evidence [13,14] indicating that surface Ti^{+3} ions play a key role in the hydrophilic properties of surfaces.

Di Valentin et al. [15] through density functional theory (DFT) calculations have shown that the presence of nitrogen atoms in the lattice of TiO_2 reduces the formation energy of oxygen vacancies.

Computational studies on Pt particles supported on titania are scarce, in contrast to the abundant literature on Au/TiO_2 [16–18]. The conclusions provided by the work of Han et al. [19], which mention the Pt_n preference to the unsaturated 2-fold-coordinated oxygen sites indicates that these sites may serve as nucleation centers for the growth of metal clusters on the oxide surface, were considered to study the Pt interaction on the stoichiometric and N-doped anatase surfaces. The increase in clustering energy with increasing size of the deposited Pt clusters indicates that the growth of Pt on this surface will lead to the formation of three-dimensional particles. Meanwhile, Gong et al. [20] assert that the Pt nucleation behavior is not affected by the presence of oxygen vacancies as if it is in the case of Au.

As far as anatase surfaces are concerned, they have not been so studied as the rutile ones. There are few studies on oxygen vacancies (V_O) on the (101) surface. Although recent work [21] concluded that the formation of vacancies in the anatase is more favorable in the bulk than on the surface, it is critical to know how the presence of these defects affects the electronic and catalytic properties of the surface [22–24].

It is worth highlighting that, in every mechanism proposed for the WGS reaction on Pt-support systems, one of the steps is the oxidation of carbon monoxide adsorbed on Pt [9]. The interest of this work is to provide theoretical and experimental results to understand how the presence of nitrogen in both, stoichiometric and reduced conditions (oxygen deficiency), affect the electronic and magnetic structures of Pt/TiO_2 system, and its influence on the adsorption of CO and its oxidation to CO_2 as possible step in the WGS or other reactions which involve CO_2 formation from CO.

2. Theoretical and experimental methods

2.1. Computational details and surface models

The calculations reported in this work were carried out in the framework of density functional theory (DFT) using the Vienna ab initio simulations package (VASP) [25–27].

Electron exchange and correlation effects are described by the generalized gradient approximation (GGA) using the functional proposed by Perdew–Wang (PW91) [28,29]. The Kohn–Sham one-electron wave functions were expanded on the basis of plane waves with kinetic energy below 400 eV. The basis of plane waves generated consider four valence electrons for Ti ($3d^34s^1$), 6 electrons for the O ($2s^2p^4$), 5 for the N electrons ($2s^2p^3$) and 10 electrons for Pt ($5d^96s^1$).

The projector augmented wave (PAW) method developed by Blöchl [30] was used to reproduce the atomic core effects in the electronic density of the valence electrons. The PAW is essentially an all-electron frozen core method combining the accuracy of all electron methods, such as the full potential linearized plane wave method, and the computational simplicity of the pseudopotential approach, especially in the implementation of Kresse and Joubert [31]. A converged ($5 \times 5 \times 1$) Monkhorst–Pack grid of special k points was adopted for integration in the reciprocal space. The Methfessel–Paxton method [32] with a smearing width of 0.20 eV was used to determine how the partial occupancies are set for each one-electron wave function. In order to evaluate the magnetic properties of the systems, the calculations were performed at the spin polarized.

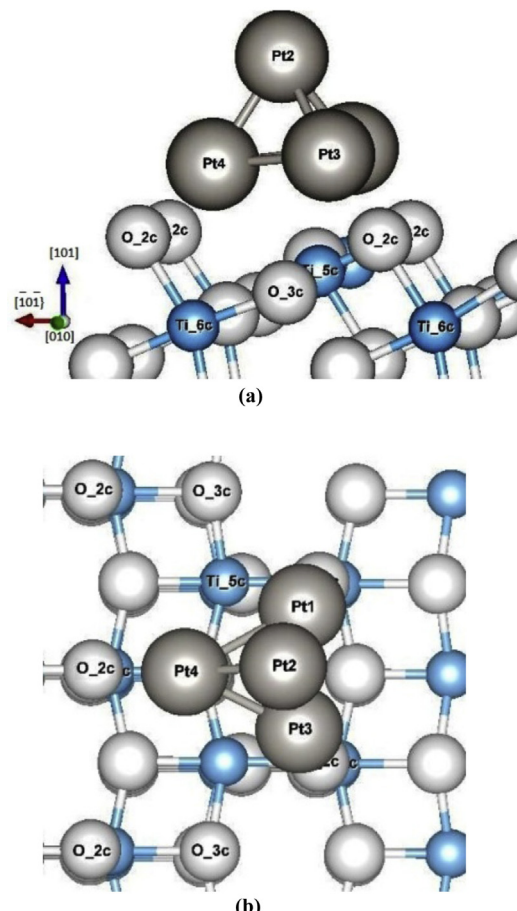


Fig. 1. Side (a) and top (b) view of anatase $\text{TiO}_2(101)$ with pyramidal Pt cluster deposited on the surface. Only the surface atoms were shown in part (b). Ti atoms on the surface consist of 5-fold (indicated Ti_{5c}) and 6-fold (Ti_{6c}), whereas the surface O atoms comprise 2-fold (O_{2c}) and 3-fold (O_{3c}). (For interpretation of color in this figure legend, the reader is referred to the web version of this article.)

The energy convergence criterion used was 0.1 meV and the value of Hubbard coefficient [33] for corrections of Coulomb interactions of the Ti d electrons was optimized to a value of 8 eV [34]. In this work, we use the Dudarev approach [35] implemented in the Vienna Ab-Initio Simulation Package (VASP) through careful selection of U, achieving excellent matches with the experimental band gap and bulk modulus measured for the systems investigated.

Some electronic characteristics as the local density of orbital states (LDOS) and the charges of the ions using Bader approach [36] were evaluated.

For calculations, the $\text{TiO}_2(101)$ anatase surface was represented with a slab containing three layers of atoms, each consisting of three atomic planes; the first and the third formed by bridges oxygens and the second one, by two rows of titaniums and oxygens. The optimized values of cell parameters are: $a = 5.44 \text{ \AA}$, $b = 3.78 \text{ \AA}$ and $c = 25.64 \text{ \AA}$ where a vacuum of 13.21 \AA was considered.

The metal–oxide interaction was modeled by placing four Pt atoms on the surface; after relaxation, the final structure was a Pt pyramidal cluster as illustrated in Fig. 1(a and b). A subsurface oxygen atom was replaced by a nitrogen atom corresponding to 0.76 wt% to represent the N doped systems ($\text{N}-\text{TiO}_2$ and Pt/N-TiO_2) (Fig. 2a), according to previous results indicating that this is the most stable position [37].

The analysis was completed studying the two systems with vacancies obtained by removing an oxygen atom (V_O) from the sur-

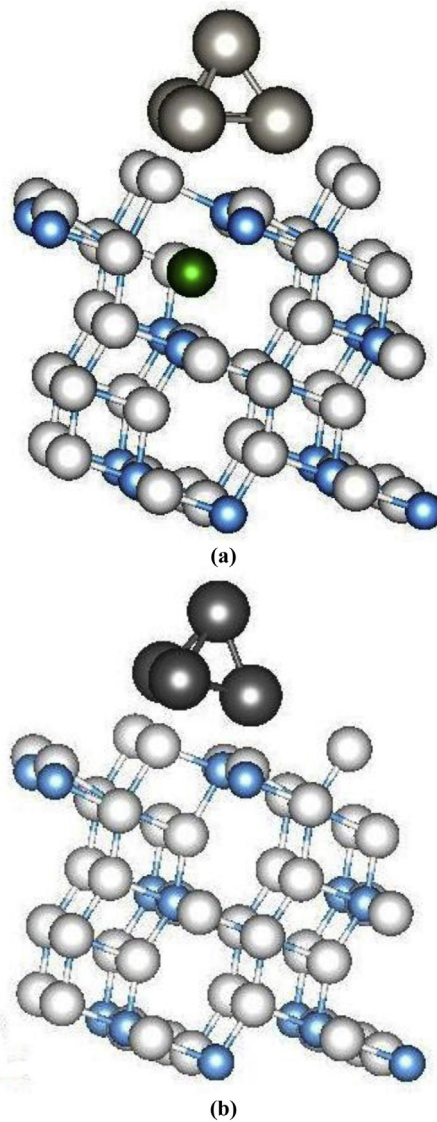


Fig. 2. Side view of anatase Pt/N-TiO₂(101) (a) and Pt/TiO₂(101)+V₀ (b). Here are depicted as examples only two of all cases studied. Blue, white, green and grey balls represent the Ti, O, N and Pt atoms, respectively. (For interpretation of the references to color in this figure legend, the reader is referred to the web version of this article.)

faces of Pt/TiO₂ (identified as Pt/TiO₂+V₀) (Fig. 2b) and Pt/N-TiO₂ (Pt/N-TiO₂+V₀).

The corresponding formation energies of the systems were computed from the respective total energies using the following equations:

$$E_{\text{for}}[\text{TiO}_2(101)+\text{V}_0] = E[\text{TiO}_2(101)+\text{V}_0] - E[\text{TiO}_2(101)] + \frac{1}{2}E_{\text{O}_2} \quad (1)$$

$$E_{\text{for}}[\text{N}-\text{TiO}_2(101)] = E[\text{N}-\text{TiO}_2(101)] - E[\text{TiO}_2(101)] - \frac{1}{2}E_{\text{N}_2} + \frac{1}{2}E_{\text{O}_2} \quad (2)$$

$$E_{\text{for}}[\text{N}-\text{TiO}_2(101)+\text{V}_0] = E[\text{N}-\text{TiO}_2(101)+\text{V}_0] - E[\text{TiO}_2(101)] - \frac{1}{2}E_{\text{N}_2} + E_{\text{O}_2} \quad (3)$$

$$E_{\text{for}}[\text{Pt}/\text{TiO}_2(101)] = E[\text{Pt}/\text{TiO}_2(101)] - E[\text{TiO}_2(101)] - E_{\text{Pt}} \quad (4)$$

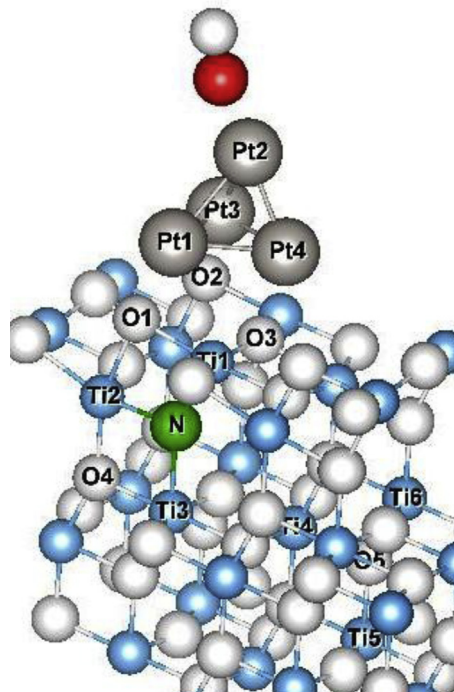


Fig. 3. CO adsorbed on Pt/N-TiO₂(101)+VO (C in red, O in white, N in green, Ti in blue, Pt in gray). Atoms numbers correspond to Table 1. (For interpretation of the references to color in this figure legend, the reader is referred to the web version of this article.)

$$\begin{aligned} E_{\text{for}}[\text{Pt}/\text{N}-\text{TiO}_2(101)] &= E[\text{Pt}/\text{N}-\text{TiO}_2(101)] - E[\text{TiO}_2(101)] \\ &\quad - \frac{1}{2}E_{\text{N}_2} + \frac{1}{2}E_{\text{O}_2} - E_{\text{Pt}} \end{aligned} \quad (5)$$

$$\begin{aligned} E_{\text{for}}[\text{Pt}/\text{TiO}_2(101)+\text{V}_0] &= E[\text{Pt}/\text{TiO}_2(101)+\text{V}_0] - E[\text{TiO}_2(101)] \\ &\quad + \frac{1}{2}E_{\text{O}_2} - E_{\text{Pt}} \end{aligned} \quad (6)$$

$$\begin{aligned} E_{\text{for}}[\text{Pt}/\text{N}-\text{TiO}_2(101)+\text{V}_0] &= E[\text{Pt}/\text{N}-\text{TiO}_2(101)+\text{V}_0] - E[\text{TiO}_2(101)] \\ &\quad - \frac{1}{2}E_{\text{N}_2} + E_{\text{O}_2} - E_{\text{Pt}} \end{aligned} \quad (7)$$

where E_{for} is the corresponding formation energy obtained for each system considered, E_{N_2} is the total energy of nitrogen gas, E_{O_2} is the total energy of oxygen gas and E_{Pt} is the Pt total energy obtained from Pt relaxed cluster calculation (4 atoms per cell). All energy values correspond to optimized systems.

The study of the carbon monoxide adsorption was done placing the adsorbate in one side of the slab on an optimized pyramidal cluster of four Pt atoms deposited on anatase surface (Fig. 3). Its geometry was allowed to optimize completely together with the Pt cluster and the top layer of the surface; the other two layers of the slab were left fixed in the position of the pre-optimized surface. The method used to optimize the titania-Pt system is the one which best represent the experimental impregnation technique of substrate with platinum employed in this work. In order to minimize the interaction between adsorbates and represent experimental concentration of N-doped, a (2×2×1) super-cell was used.

The corresponding CO adsorption energies were obtained using the following equation:

$$E_{\text{ads}} = E_{\text{CO/sys}} - (E_{\text{CO}} + E_{\text{sys}}) \quad (8)$$

where E_{ads} is the CO adsorption energy, $E_{\text{CO/sys}}$ is the total energy of the system with CO adsorbed, E_{CO} is the total energy of carbon

monoxide gas and E_{sys} is the total energy corresponding to systems: Pt/TiO₂, Pt/TiO₂ + V_O, Pt/N-TiO₂ and Pt/N-TiO₂ + V_O.

2.2. Set-up experimental

Experimental tests were carried out using a commercial sample of TiO₂ (Hombifine N, Sachtleben Chemie) as support. Nitrogen-doped TiO₂ was prepared by precipitacion according to Wang et al. [38]. Titanium (IV) isopropoxide Ti(OCH(CH₃)₂)₄ (Aldrich 97%) was added dropwise into H₂O under continuous stirring obtaining a homogeneous colloidal solution. Concentrated nitric acid was then added slowly to the sol to achieve a translucent solution. After vigorous stirring for 30 min, aqueous ammonium hydroxide solution (Cicarelli 28%) was added drop by drop into the solution until pH 9. The resulting precipitate was filtered and washed thoroughly with deionized water and dried in the air at room temperature. Then, the dried precipitate was calcined in air at 623 K for 4 h.

Pt-supported samples were prepared by incipient-wetness impregnation of supports at 303 K with aqueous solutions of tetramine platinum nitrate, Pt(NH₃)₄(NO₃)₂ (Aldrich, 99.99%). After impregnation, samples were dried overnight at 363 K and then reduced at 473 K in H₂ for 2 h.

The crystalline structure and crystal size of supports were determined by X-ray diffraction (XRD) in the range of $2\theta = 20\text{--}80^\circ$, using a Shimadzu XD-D1 diffractometer and Ni filtered Cu K α radiation ($\lambda = 1.540 \text{ \AA}$). Crystallite sizes were calculated using the Debye Scherrer equation. BET surface areas (S_g) were measured by N₂ physisorption at its boiling point in a Micromeritics Accusorb 2100 E sorptometer. Prior to N₂ physisorption, samples were degassed for 3 h at 523 K. Diffuse reflection spectra of the supports, TiO₂ and N-TiO₂, were obtained using a UV-visible diffuse reflectance spectrometer (PerkinElmer Lambda 40) and Spectralon standard was employed to measure the reference line. The Pt loadings were measured by atomic absorption spectroscopy. The platinum dispersion (D_{Pt}) on Pt/TiO₂ and Pt/N-TiO₂ samples was determined by H₂ chemisorption at 298 K using a conventional vacuum unit. Catalysts were reduced in H₂ at 473 K for 2 h and then outgassed for 2 h at the same temperature prior to performing gas chemisorption experiments. Hydrogen uptake was determined using the double isotherm method [39,40].

CO adsorption on Pt-based catalysts was studied by diffuse reflectance infrared Fourier transform spectroscopy (DRIFTS) experiments which were carried out in a Shimadzu IRPrestige-21 spectrophotometer, equipped with an in-situ high-temperature/high pressure SpectraTech cell and a liquid nitrogen-cooled MCT detector. The sample holder, a ceramic crucible containing a heating resistor and a thermocouple, was placed inside a dome with CaF₂ windows. The spectral resolution was 4 cm⁻¹ and 40 scans were added. The gas flow rates were always 60 mL/min. Samples ($W = 50 \text{ mg}$) were initially reduced in H₂ at 473 K for 30 min, then treated 10 min in Ar at 573 K and finally cooled down in Ar to 303 K. Background spectra of the samples in Ar were taken from 573 to 303 K, at 50 K intervals. A flow of 5% CO in N₂ was admitted at 303 K and the sample spectrum collected. Then the sample temperature was raised to 573 K in Ar, at 50 K intervals, for collecting the respective DRIFT spectra. The results given herein are difference spectra, where the background spectra of the sample in Ar served as the reference.

In order to gain more information related to the role of the support on CO oxidation, additional tests were carried out in a plug-flow fixed-bed reactor (Pyrex, 0.8 cm ID) fed with a gaseous stream 1% CO/N₂ at 573 K and 101.3 kPa. The reactor outlet, containing the reaction product (CO₂) and non-converted reactant (CO), was analyzed using a gas chromatograph Shimadzu 2014 equipped with a flame ionization detector and a Supelco SP1700 column. Before gas chromatographic analysis, the reaction products were sepa-

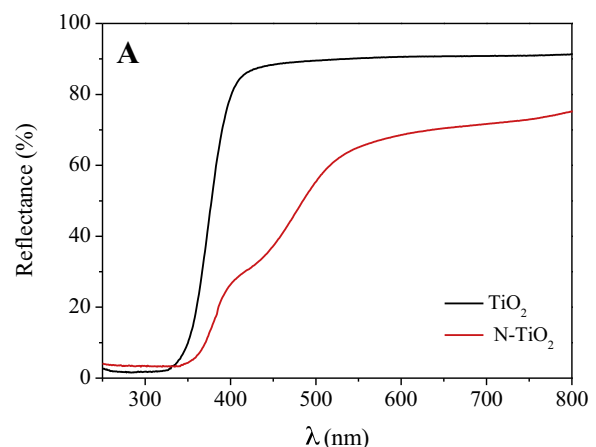


Fig. 4. Diffuse reflectance spectra of TiO₂ and N-TiO₂.

rated and CO and CO₂ completely converted to CH₄ by means of a methanation catalyst (Ni/Kieselghur) operating at 673 K. The CO conversion was calculated as: $X_{\text{CO}}(\%) = \frac{n_{\text{CO}_2}}{(n_{\text{CO}} + n_{\text{CO}_2})} \times 100$ where n_{CO} and n_{CO_2} are the outlet mole flows of CO and CO₂ (mol/min), respectively. The CO conversion definition involves CO₂ moles formed as reaction product and remanent CO at the reactor outlet. Moreover, the carbon balance result was 100 which means that unconverted CO is outflowing the reactor.

3. Results

3.1. Theoretical results

3.1.1. TiO₂(101), TiO₂(101)+V_O, N-TiO₂(101) and N-TiO₂(101)+V_O

In this section we present the salient features of pure TiO₂(101) surface and also analyze how the N-doped and oxygen deficiency (i.e., presence of oxygen vacancy, V_O) affect the electronic and geometric properties of the surface. The main results related to distances and charges are summarized in Table 1.

No reconstruction was observed in the relaxed TiO₂(101) surface, but a high value of magnetic moment (8 μ_{B} /unit cell) is appreciated (Table 2). The bi-coordinated oxygen (O.2c) located on the step, is more oxidized ($-1.31e$) than the oxygen atoms of the sublayer ($-1.42e$). Even further, compared with the bulk structure, the charges of the surface are transferred to the body as has been observed in other studies [41] (see Table 1). In particular, the local average magnetic moment of the Ti³⁺ ions, result of the subcoordination of Ti surface, is 0.96 μ_{B} per ion.

Regarding bulk titania (anatase), the conduction band (CB) of the (101) surface is widened by 77% due to the presence of the O.2c eigenstates. The density of states of the pure surface has an occupied state in the band gap (BG) localized at 1.46 eV with respect to the conduction band bottom (CB) (Table 2 and Fig. 4). These observations about the appearance of localized states in the BG product of the presence of Ti³⁺ ions are consistent with those obtained in the work of Portillo Velez et al. [42].

As it is known, an oxygen vacancy converts two Ti⁴⁺ ions into two Ti³⁺ ions, which also results in a local average magnetic moment of 0.89 μ_{B} per Ti³⁺, in concordance with the value of 1 μ_{B} per Ti³⁺ obtained by Yang et al. [43] for anatase phase. Additional analysis of the local density of states shows that the states of the Ti near to the vacancy, migrates to the valence band, widening it by 0.37 eV.

According to Eq. (2), replacing an oxygen atom by a nitrogen atom to dope the surface, has an energy cost of -1.10 eV . The pres-

Table 1

Bader charges and principal distances between atoms theoretically calculated.

Systems	Atoms	Dist (Å)	Charges (e)								
			N	Ti*	O*	Ti**	O**	Ti bulk	O bulk	Ti#	O#
TiO ₂ (bulk)	Ti–O	2.03 (ap) 2.02 (eq)	--	--	--	--	--	2.75	-1.37	--	--
TiO ₂ (101)	O5–Ti6	1.93	--	2.76 (Ti1) (O1/2/3)	-1.31	--	--	2.76 (Ti6) 2.78 (Ti4) 2.74 (Ti5)	-1.42 (O5)	--	--
	O5–Ti4	1.97									
	O5–Ti5	1.93									
TiO ₂ (101)+V _O	O5–Ti6	1.93	1.97	--	2.30 (Ti1) (O1)	-1.28	--	2.74 (Ti6)	-1.45 (O5)	2.29 (Ti1)	-1.28 (O1)
	O5–Ti4	1.93				-1.28 (O2)	--	2.79 (Ti4)			
	O5–Ti5					-1.48 (O3)	--	2.29 (Ti5)			
N–TiO ₂ (101)	N–Ti1	2.02	-1.59	2.7 (Ti1)	-1.26 (O1)	2.7 (Ti1)	-1.37 (O4)	2.80 (Ti6) 2.79 (Ti4) 2.39 (Ti5)	-1.36 (O5)	--	--
	N–Ti3	1.93									
	N–Ti2	2.03				-1.27 (O2)	2.77 (Ti3)				
	O5–Ti6	1.93				-1.26 (O3)	2.71 (Ti2)				
N–TiO ₂ (101)+V _O	N–Ti1	2.06	-1.76	2.26 (Ti1)	-1.30 (O1)	2.26 (Ti1)	-1.42 (O4)	2.81 (Ti6) 2.79 (Ti4) 2.29 (Ti5)	-1.37 (O5)	2.26 (Ti1)	-1.28 (O1)
	N–Ti3	1.93				-1.28 (O2)	2.77 (Ti3)				
	N–Ti2	1.94				-1.47 (O3)	2.61 (Ti2)				
	O5–Ti6	1.93									
	O5–Ti4	1.97									
	O5–Ti5	1.93									

The corresponding atoms numbers are indicated in the Fig. 3. The charges nomenclature used is the following: N (nitrogen), Ti* (Ti atoms surface), O* (O atoms surface), Ti** (Ti atoms bonded to N atom); O** (O atoms nearby N atom), Ti and O bulk (Ti y O away from the defects), Ti# (Ti atoms nearby oxygen vacancy) and O# (O atoms nearby oxygen vacancy). Ap: apical Ti–O distance, eq: equatorial Ti–O distance.

Table 2

Main features of the electronic structure of systems.

System	E _{for} (eV)	μ (μ _B /cell)	BG (eV)	VB (eV)	CB (eV)	BG states (eV)
TiO ₂ (anatase)	---	0.0	3.21	4.53	2.06	----
TiO ₂ (101)	---	8.0	2.10	5.11	3.65	1.46
TiO ₂ (101)+V _O	+2.50	6.0	2.01	5.48	3.66	1.46–1.74
N–TiO ₂ (anatase)	---	2.87				
N–TiO ₂ (101)	-1.10	5.0	1.12	7.48	2.99	0.19–1.03
N–TiO ₂ (101)+V _O	0.57	9.0	1.92	5.57	3.65	1.55
Pt/TiO ₂ (101)	-4.31	6.0	2.75	5.42	2.94	0.55–0.83–1.84–2.20–2.57
Pt/TiO ₂ (101)+V _O	-1.56	10.0	3.00	5.40	2.61	0.47–1.21–1.40–1.77–2.33–2.61
Pt/N–TiO ₂ (101)	-6.66	3.0	2.01	5.39	3.66	0.18–0.37–0.82–1.10–1.83
Pt/N–TiO ₂ (101)+V _O	-3.99	5.0	2.39	5.24	3.22	0.37–0.74–1.10–1.84–2.21

BG: band gap, VB: valence band width, CB: conduction band width, BG states: states in the BG located from the base of CB. E_{for}: corresponding formation energies of the systems studied calculated using the equations indicated in the text (see Section 2.1). The values related to bulk anatase (undoped and N-doped) are highlighted in gray.

ence of nitrogen produces a decrease of 37.5% in the value of the magnetic moment per unit cell (from 8 μ_B to 5 μ_B).

In particular, N–Ti1 and N–Ti2 distances are elongated with respect to the O–Ti distances as can be seen in Table 1. This can be explained considering that the N has a lower electronegativity than O. When the bond is elongated, Ti charges are reduced acquiring 0.023e on average (Ti** in Table 1). However, the nitrogen becomes negatively charged (-1.59e), being this charge greater than that of oxygen it replaces (-1.42e).

When the surface is doped the generation of an oxygen vacancy varies significantly the formation energy from -1.10 eV to 0.57 eV (Table 2). This value is considerably lower than that calculated for the formation energy of an oxygen vacancy in the pure surface (2.50 eV) obtained from the Eq. (1). Our results reinforce the hypothesis proposed by Batzill et al. [44], who argue that the stabilization of vacancies in coexisting with N as a dopant, is the result of charge compensation where the N⁻³ is stabilized by the electrons from the O vacancy.

This interpretation is in agreement with the observations relating to changes in the value of magnetic moment. Whereas the nitrogen causes a decrease in the spin magnetic moment value with

respect to the case of the surface undoped (as mentioned above), the presence of N in the surface with oxygen vacancies, increases the spin magnetic moment of the cell (9 μ_B/cell unit) if compared with the case of TiO₂(101)+V_O surface (6 μ_B/cell unit).

The BG values calculated for anatase bulk (undoped and N-doped) are showed in Table 2. A BG narrowing of 10.6% is observed for the N-doped anatase. Similar conclusions were experimentally obtained from the analysis of the UV-visible diffuse reflection spectra (DRS) of N-doped and undoped TiO₂ (Fig. 4). The band gap values were determined by plotting the [hvF(R)]^{1/2} against hv, where F(R)=(1-R)²/2R was Kubelka–Munk function (Fig. 5), applying the Tauc relational expression [45,46]. The band gap of TiO₂ sample was 3.28 eV whereas doping the system with N reduced the band gap to 3.02 eV (8%).

From the analysis of the DOS curves of N-doped surface (Fig. 6a), it may be mentioned that in comparison with the pure surface, the CB is reduced in contrast to VB which widens due to the presence of localized N 2p states. The dopant induces a reduction of BG (46%) and contributes with localized states at 0.19 eV and 1.03 eV from the CB bottom.

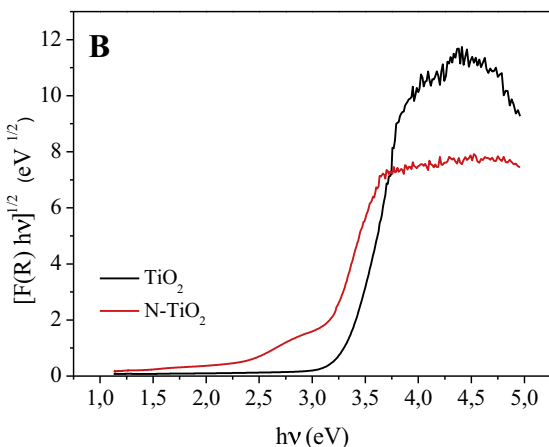


Fig. 5. Plots of $[h\nu F(R)]^{1/2}$ against $h\nu$ of TiO_2 and $N-TiO_2$.

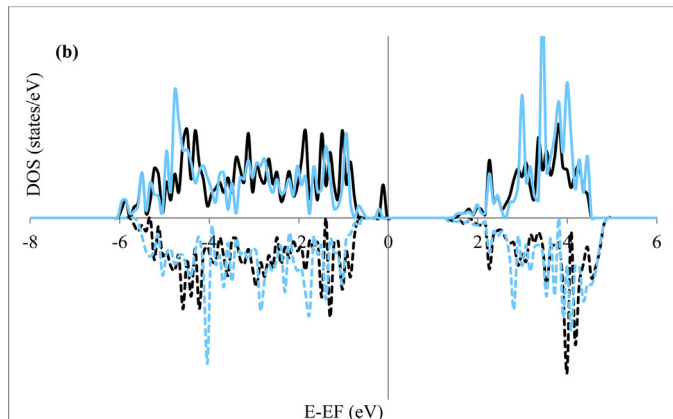
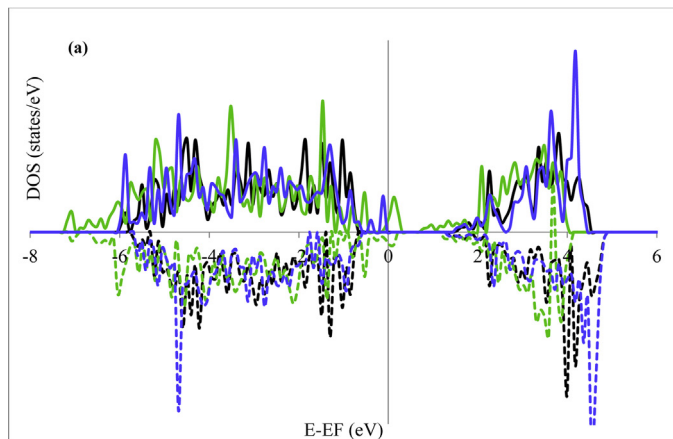


Fig. 6. (a) DOS curves of undoped anatase surface (black curve), N-doped surface (green curve) and oxygen-deficient surface (blue curve). (b) DOS curves of oxygen-deficient doped surface (turquoise curve). The spin-down cases were plotted as negative values. (For interpretation of the references to color in this figure legend, the reader is referred to the web version of this article.)

Regarding the study of oxygen-deficient doped surface, the analysis of the DOS curves (Fig. 6b) shows a state located in the BG at 1.55 eV relative to the base of the CB. Compared with the surface undoped, a decrease of BG width and increase of BV width due to the presence of states of N are observed, in agreement with that observed by Chen et al. [47]. However, if we compare with the doped surface, the situation is different: the BG width increases

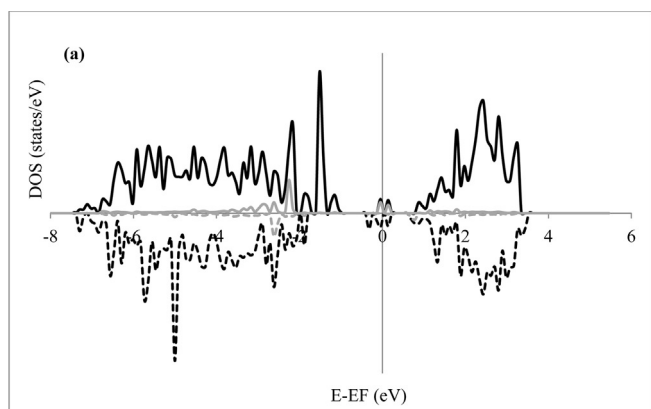


Fig. 7. (a) DOS curves of $Pt/TiO_2(101)$ surface (black curve) and local density of states (LDOS) of Pt atom (gray curve). (b) DOS curves of $Pt/N-TiO_2(101)$ surface (black curve) and LDOS of Pt atom (black curve) and LDOS of N atom (green curve). The spin-down cases were plotted as negative values. (For interpretation of the references to color in this figure legend, the reader is referred to the web version of this article.)

and the vacancy formation produce the narrowing of the VB and the increase in the CB width.

3.1.2. $Pt/TiO_2(101)$, $Pt/N-TiO_2(101)$, $Pt/TiO_2(101) + V_O$ and $Pt/N-TiO_2(101) + V_O$

In this section we present the results obtained by depositing a nano-cluster of Pt on pure and doped (101) surface following the procedure explained in Section 2.

The addition of a tetrahedral cluster of four Pt atoms on the surface has a cost of -4.31 eV and -6.66 eV for stoichiometric and N-doped surfaces, respectively, values obtained using Eqs. (4) and (5).

Depositing Pt on pure (101) surface increases the width of the band gap of 2.10–2.75 eV. The valence band widens 0.31 eV and the conduction band narrows 0.71 eV. In the corresponding DOS curve can be seen five states, including four occupied, due to the adsorption of Pt (Fig. 7a and Table 2). Those closest to the BV states are formed mainly by hybridization $Ti\ 3d - O\ 2p$. The Fermi level remains unchanged with respect to the pure surface but when the Pt is adsorbed, the bands are shifted to lower values of energy.

When Pt is deposited on the doped surface ($Pt/N-TiO_2(101)$), the width of the band gap also increased (0.89 eV) when compared to the surface $N-TiO_2(101)$ (Table 2). The states located in the BG, migrates to the BC and the contribution of these Pt states increases in importance with respect to the addition of Pt on the undoped surface (Fig. 7b).

In all cases studied in this work, when Pt is present on the surface, the BG increases possibly due to the repulsion between d and f orbitals of Pt with d orbitals of Ti.

The value of the spin magnetic moment of pure surface decreases about $2 \mu\text{B}$ by the presence of Pt cluster (Table 2). It is noteworthy that this situation is the same when the surface is doped with N because the corresponding value of the magnetic moment of $5 \mu\text{B}$ decreases to $3 \mu\text{B}$ when Pt is on the surface.

According to our findings, the platinum promotes oxidation of the pure surface oxygens ($-1.31e$ to $-1.24e$) and reduce the nearest Ti (2.66 – $2.76e$) indicated as Ti^* in Table 3. The average platinum charge in contact with the surface (Pt1, Pt3 and Pt4) is $0.08e$, relatively minor and opposite sign to Pt2 charge, which is $-0.18e$. In particular, Pt4 presents greater difference in charge with respect to the remaining contact surface Pt (P1 and Pt3), possibly by its location in hollow site.

The addition of Pt to N-doped surface (Pt/N-TiO₂(101)) promotes oxidation of the surface oxygens ($-1.26e$ to $-1.22e$) and reduces the nearest Ti (2.67 – $2.70e$). In this case, the average platinum charge in contact with the surface (Pt1, Pt3 and Pt4) is $0.18e$, a greater value than the acquired when the surface is not doped. It is noteworthy that the nitrogen becomes more negative ($-1.74e$) than when there are no platinum on the surface ($-1.59e$). Newly, Pt4 presents greater difference in charge with respect to the remaining contact surface P1 and Pt3.

What new features does the presence of oxygen vacancies provide to those recently studied in the previous section? First, we note that the presence of nitrogen stabilizes the Pt/system from -3.99 eV to -1.56 eV (Table 2) values obtained using Eqs. (6) and (7).

If we compare with the corresponding systems without vacancies, we note that the valence bands remain unchanged unlike the BG which expands.

Pt adds states mostly occupied in the band gap, which reduce the energy required for activation of the titania. When the system is also doped, N-states hybridize with those of the Ti^{+3} produced by the oxygen vacancy (Fig. 8).

Once again, as in the N-doped structures, the characteristic referred to the increase in the value of the magnetic moment when a particular system is oxygen-deficient is repeated (Table 2).

With respect to the charge values, the concomitant presence of N and oxygen vacancies generally oxidized the Pt (except Pt4). The oxygen atoms coordinated with Pt are oxidized in the presence of nearby vacancies. Ti and O near the vacancy (marked with # in Table 2) also undergo oxidation because of the Pt presence on the surface.

3.1.3. CO adsorbed on $\text{Pt/TiO}_2(101)$, $\text{Pt/TiO}_2(101) + \text{V}_0$, $\text{Pt/N-TiO}_2(101)$ and $\text{Pt/N-TiO}_2(101) + \text{V}_0$

Many catalytic reactions involve the oxidation reaction of CO to CO₂ as intermediate step among them the WGS can be highlighted. In the work of Vignatti et al. [9], among all the mechanisms proposed for Pt supported on reducible and non-reducible oxides as catalysts, CO is always adsorbed on Pt. In particular, Pt/TiO₂ has been reported as a bifunctional catalyst at low temperatures where the reaction takes its higher performance, because the CO is adsorbed on Pt and the oxide activates H₂O. Specifically, in one of the most viable redox route, the CO adsorbed on the Pt could be oxidized to CO₂ by O atoms of the support surface. It is therefore desirable that the catalyst (Pt/TiO₂) abides in a reducible state as much as possible in order to favor CO conversion.

In this section we present the theoretical results obtained by absorbing CO on the systems analyzed in Section 3.1.2. The main results related to distances, angles, magnetic moments, charges and CO vibrational frequencies are summarized in Table 4. The most representative systems atoms and adsorbate were selected. The

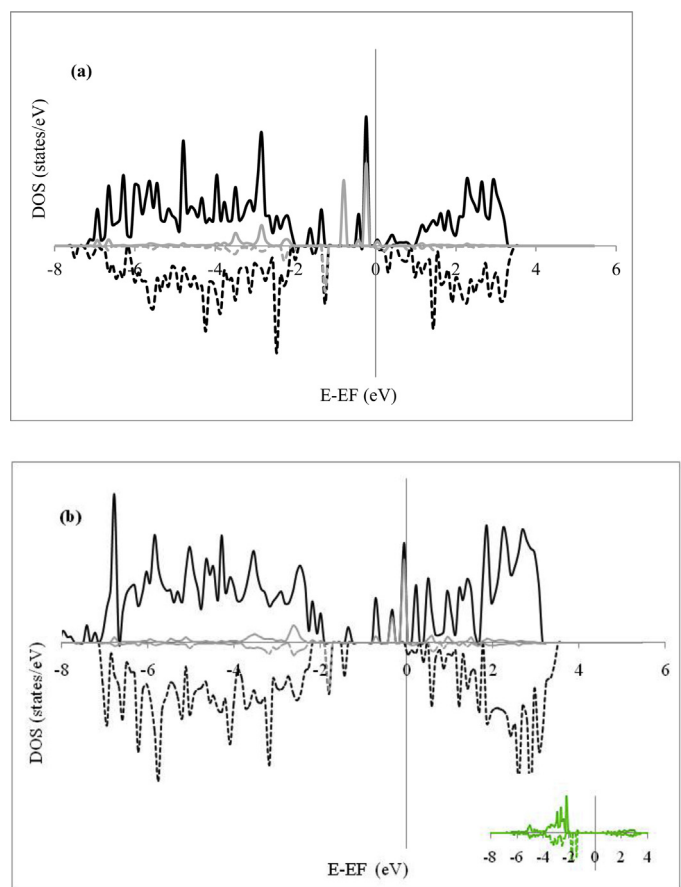


Fig. 8. (a) DOS curves of $\text{Pt/TiO}_2 + \text{V}_0$ surface (black curve) and local density of states (LDOS) of Pt atom (gray curve). (b) DOS curves of $\text{Pt/N-TiO}_2 + \text{VO}$ and LDOS of Pt atom (black curve) and LDOS of N atom (green curve). The spin-down cases were plotted as negative values. (For interpretation of the references to color in this figure legend, the reader is referred to the web version of this article.)

corresponding CO adsorption energies were calculated using Eq. (8) and the results were included in the table.

Firstly, we analyze the CO adsorption in undoped systems. As reference the vibration frequency and C–O distance of gaseous CO (free molecule) were calculated; the obtained values are: 2128 cm^{-1} and 1.142 \AA , respectively.

As far as the CO chemisorption is concerned, the fundamental concept of back-donation introduced by Blyholder should be mentioned [48]. It was largely confirmed by other studies on various transition metal substrates that the electron back-donation from the substrate d levels to the CO $2\pi^*$ orbital is of primary importance.

In our case, back-donation implies a movement of electrons from Pt atomic orbital $5d$ to CO $2\pi^*$ antibonding orbital of CO. This causes that the charge on the Pt, particularly Pt2, become positive and the binding order in the ligand (CO) decreases, increasing the order of metal-ligand binding. This generally leads to a decrease in vibrational frequency bond measurable by IR spectroscopy. This back-donation is observed in all four cases analyzed in this work, being of greater magnitude in the $\text{Pt/TiO}_2(101) + \text{V}_0$ system (see Tables 3 and 4).

However, the analysis of the back-donation effect is complex, not only the binding of metal with CO must be considered, factors such as nitrogen presence (p -dopant type) and/or the formation of oxygen vacancies (n -dopant type) are added. According to the lost Pt2 charges values, the expected order for the Pt2-C distances would be: $\text{Pt/TiO}_2(101) + \text{V}_0 > \text{Pt/N-TiO}_2(101) > \text{Pt/N-TiO}_2(101) + \text{V}_0 > \text{Pt/TiO}_2$

Table 3

Bader charges and principal distances between atoms theoretically calculated.

Systems	Atoms	Dist (Å)	Charges (e)									
			N	Pt	Ti*	O*	Ti**	O**	Ti bulk	O bulk	Ti#	O#
Pt/TiO ₂ (101)	Pt2–Pt1	2.55	--	0.03	2.66	-1.23	--	--	2.80 (Ti6)	-1.36	--	--
	Pt2–Pt3	2.54		(Pt1)	(Ti1)				2.79 (Ti4)	(O5)		
	Pt2–Pt4	2.53		-0.18		(O1)			2.30 (Ti5)			
	Pt1–Pt3	2.57		(Pt2)		-1.23						
	Pt1–Pt4	2.90		0.03		(O2)						
	Pt3–Pt4	2.77		(Pt3)		-1.27						
	Pt1–O1	2.07		0.19		(O3)						
	Pt3–O2	2.09		(Pt4)								
Pt/TiO ₂ (101) +V _O	Pt4–O3	2.08										
	Pt2–Pt1	2.59	--	0.10	2.66	-1.24	--	--	2.78 (Ti6)	-1.35	2.66	-1.23
	Pt2–Pt3	2.59		(Pt1)	(Ti1)	(O1)			2.77 (Ti4)	(O5)	(Ti1)	(O1)
	Pt2–Pt4	2.55		-0.17		-1.24			2.24 (Ti5)			
	Pt1–Pt3	2.62		(Pt2)		(O2)						
	Pt1–Pt4	2.67		0.10		-1.36						
	Pt3–Pt4	2.67		(Pt3)		(O3)						
	Pt1–O1	2.06		-0.18								
	Pt3–O2	2.06		(Pt4)								
	Pt4–O3	2.12										
	O5–Ti6	1.93										
	O5–Ti4	1.97										
	O5–Ti5	1.93										
Pt/N-TiO ₂ (101)	Pt2–Pt1	2.57	-1.74	0.19	2.67	-1.18	2.67	-1.41 (O4)	2.81	-1.40	--	--
	Pt2–Pt3	2.53		(Pt1)	(Ti1)	(O1)	(Ti1)		(Ti6)	(O5)		
	Pt2–Pt4	2.54		-0.19		-1.23	2.77					
	Pt1–Pt3	2.51		(Pt2)		(O2)	(Ti3)		(Ti4)			
	Pt1–Pt4	2.80		0.14		-1.25	2.74					
	Pt3–Pt4	2.82		(Pt3)		(O3)	(Ti2)		(Ti5)			
	Pt1–O1	2.01		0.22								
	Pt3–O2	2.06		(Pt4)								
	Pt4–O3	2.12										
	N–Ti1	1.93										
	N–Ti3	2.10										
	N–Ti2	1.93										
	Pt2–Pt1	2.61	-1.74	0.21	2.66	-1.20	2.66	-1.40	2.80 (Ti6)	-1.36 (O5)	2.66	-1.20
Pt/N-TiO ₂ (101) +V _O	Pt2–Pt3	2.55		(Pt1)	(Ti1)	(O1)	(Ti1)	(O4)	2.77 (Ti4)		(Ti1)	(O1)
	Pt2–Pt4	2.56		-0.16		-1.23	2.73		2.28 (Ti5)			
	Pt1–Pt3	2.54		(Pt2)		(O2)	(Ti3)					
	Pt1–Pt4	2.62		0.17		-1.38	2.69					
	Pt3–Pt4	2.64		(Pt3)		(O3)	(Ti2)					
	Pt1–O1	1.98		-0.04								
	Pt3–O2	2.04		(Pt4)								
	Pt4–O3	2.13										
	N–Ti1	1.92										
	N–Ti3	2.14										
	N–Ti2	1.96										
	O5–Ti6	1.93										
	O5–Ti4	1.97										
	O5–Ti5	1.93										

The corresponding atoms numbers are indicated in Fig. 3. The charges nomenclature used is the following: N (nitrogen), Ti* (Ti atoms coordinated to Pt atoms), O* (O atoms coordinated to Pt atoms), Ti** (Ti atoms bonded to N atom); O** (O atoms nearby N atom), Ti and O bulk (Ti y O away from the defects), Ti# (Ti atoms nearby oxygen vacancy) and O# (Ti atoms nearby oxygen vacancy). Ap: apical Ti–O distance, eq: equatorial Ti–O distance.

which is not satisfied. This order is neither verified when observing the C charges. Based on the values presented in Tables 3 and 4, our hypothesis is that electrons donated by Pt2 would be acquired by the oxygen of CO, increasing the ionic character of the bond and increasing the C–O distances.

What changes are observed when the surface is doped? The results confirm that the adsorption of CO is favored when the surface is N-doped by 0.06 eV (Table 4), relative to the value obtained for undoped system. Furthermore, the Pt-surface bonding is strengthened, by observing for example, that the distances between the Pt in contact with the surface (Pt1–Pt3–Pt4) and the oxide oxygen shorten on average 0.07 Å. These results reinforce the findings presented in the previous section related to the presence of N in the Pt/TiO₂(101) system, stabilizes it; one possible explanation is that, since the N (oxidation state N⁻³) substitutes an oxygen of titania which oxidation state is O⁻², attracts electrons of Pt oxidizing them on average 0.10e.

However, if we include oxygen vacancies in the system, the nitrogen destabilizes it, increasing the CO bond order, decreasing strongly the energy released in the absorption of CO (-1.77 a -1.67 eV) and increasing the C–Pt2 distance. Besides, the decreasing C–O distance in the Pt/N-TiO₂ + V_O system in comparison with Pt/TiO₂ + V_O system, indicates greater hybridization between them. In order to assess the changes in the electron density, the corresponding LDOS (Fig. A.1-Supplementary data) and isosurfaces of charge density difference between distinct systems were plotted using VESTA [49] (Fig. A.2-Supplementary data). From charge density differences shown in Fig. A.2, the case (c) should be emphasized. The absence of oxygen vacancies does not favor the polarization of the CO molecule observed in the other cases. The covalent character of the CO bond in this situation is preserved, decreasing its activity compared to the other situations studied.

Supplementary material related to this article found, in the online version, at <http://dx.doi.org/10.1016/j.molcata.2015.06.024>

Table 4

Main results related to distances, angles, magnetic moments and Bader charges theoretically calculated.

Distances (Å)				
Atoms	Pt/TiO ₂ (101)	Pt/N-TiO ₂ (101)	Pt/TiO ₂ (101)+V _O	Pt/N-TiO ₂ (101)+V _O
C–O	1.167	1.168	1.170	1.165
C–Pt2	1.872	1.881	1.868	1.875
Pt2–Pt3	2.689	2.647	2.728	2.747
Pt2–Pt4	2.523	2.525	2.500	2.489
Pt2–Pt1	2.683	2.674	2.720	2.713
Pt3–O2	2.121	2.092	2.068	2.045
Pt1–O1	2.067	2.007	2.067	1.974
Pt4–O3	2.111	1.998	2.067	2.291
Pt2–Ti1	4.861	4.899	4.802	4.940
Angles (°)				
O–C–Pt2	170.08	169.36	167.88	166.80
Magnetic moment (μ_B /cell)				
CO/	2.0	7.0	6.0	5.0
Charges (e)				
C	1.566	1.638	1.643	1.659
O	-1.841	-1.889	-1.889	-1.865
q _{CO} net	-0.275	-0.251	-0.246	-0.206
Pt1	0.026	0.197	0.099	0.222
Pt2	0.125	0.129	0.159	0.145
Pt3	0.016	0.103	0.109	0.172
Pt4	0.079	0.103	-0.302	-0.205
O1	-1.235	-1.177	-1.225	-1.173
O2	-1.233	-1.216	-1.224	-1.223
O3	-1.282	-1.413	-1.387	-1.378
Ti1	2.668	2.676	2.691	2.673
N	---	-1.748	---	-1.758
E_{ads} (eV)				
CO/	-1.90	-1.96	-1.77	-1.67
ν_{CO} (cm ⁻¹)				
CO/	1986	1982	2007	2018

The most representative systems atoms and adsorbate were selected. The corresponding CO adsorption energies were calculated using Eq. (8) (see text). The corresponding atoms numbers are indicated in Fig. 3.

Concerning the results related to the spin magnetization, nitrogen doping decreases the value of the magnetic moment of the cell (see Table 2), either in presence or absence of oxygen vacancies, except in the most unstable systems regarding their energy of formation (TiO₂+V_O and N-TiO₂+V_O).

When the system is N-doped, the average platinum distance in contact with the surface is shortened and the Pt–C–O angle is shrinking (from 170.08° to 169.36°, see Table 4) favoring this geometry, the reaction between CO and one O surface to form CO₂. Moreover, this theory is strengthened by the higher C positivity in the indicated system (1.659e) compared to other systems (Table 4).

3.2. Experimental results

As far as physicochemical properties of Pt-based catalysts used in experimental studies are concerned, both samples, Pt/TiO₂ and Pt/N-TiO₂, showed similar values of specific surface (S_g) areas, 186 m² g⁻¹ and 181 m² g⁻¹, respectively. Accessible metal fractions (D_{Pt}) determined by H₂ chemisorption at 298 K on Pt/TiO₂ and Pt/N-TiO₂ were 11 and 25%, respectively. X-ray diffraction patterns of the catalysts exhibited the diffraction lines of anatase phase (not shown in this work). The average crystal size of the catalyst without N was 120 Å whereas in the case of the N-doped sample the crystal size was 99 Å. No diffraction line attributed to crystalline phases of Pt was detected probably because of low metal loadings.

Figs. 9 and 10 present the DRIFTS spectra obtained on stream during CO (5%)/N₂ adsorption at 303 K on Pt/TiO₂ and Pt/N-TiO₂, respectively (spectra a). Moreover, the figures show the spectra recorded after purging both systems in Ar at increasing temperatures from 303 to 573 K (Fig. 9, spectra b–e and Fig. 10,

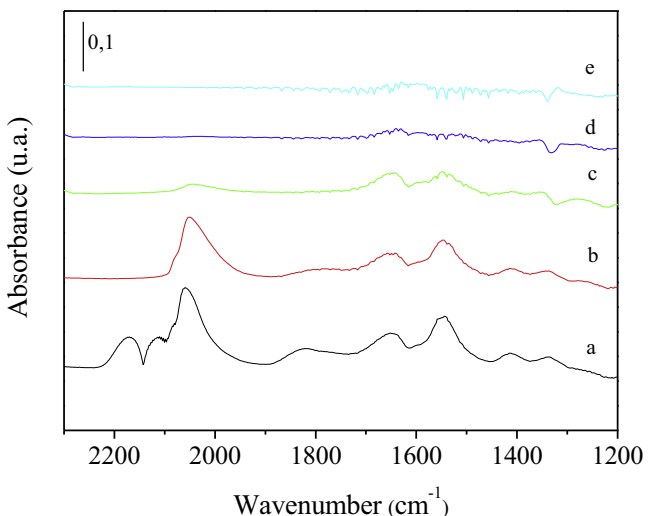


Fig. 9. In situ DRIFTS spectra on CO(5%)/N₂ at 303 K on Pt/TiO₂ (a); purged in Ar at 303 K (b); 323 K (c); 373 K (d) and 423 K (e).

spectra b–h). As it is well-known, CO adsorption at 303 K (spectra a) shows two bands corresponding to gaseous CO detected in the 2175–2112 cm⁻¹ region. Furthermore, both catalysts showed bands located between 2085 and 2040 cm⁻¹ which are assigned to linear bonded CO on Pt⁰ (Pt⁰–C) [50,51] during CO adsorption and after purging in Ar at 303 K (spectra a and b). In particular, on Pt/TiO₂, a peak that could be attributed to CO adsorbed on Pt⁰ in bridge form appeared at 1830 cm⁻¹ [52] (Fig. 9, spectra a and

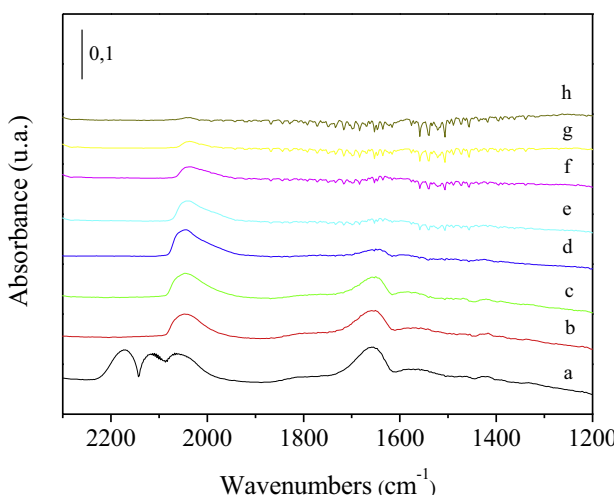


Fig. 10. In situ DRIFTS spectra on CO(5%)/N₂ at 303 K on Pt/N-TiO₂ (a); purged in Ar at 303 K (b); 323 K (c); 373 K (d); 423 K (e); 473 K (f); 523 K (g) and 573 K (h).

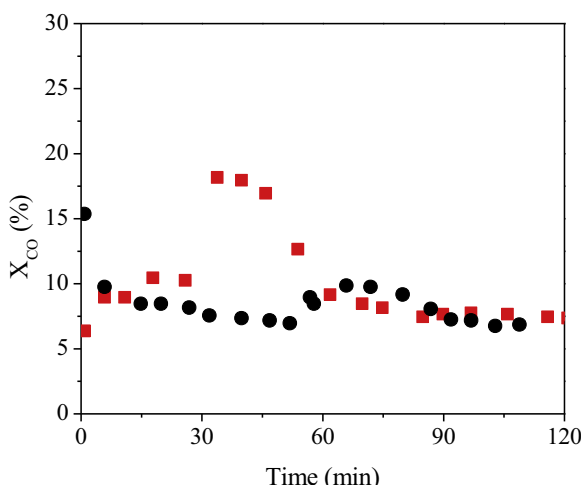


Fig. 11. CO conversion as a function of time in absence of H₂O: Pt/TiO₂ (black circles) and Pt/N-TiO₂ (red square) (1% CO in N₂, T = 573 K, P = 101.3 kPa, W_{cat} = 100 mg). (For interpretation of the references to color in this figure legend, the reader is referred to the web version of this article.)

b). Both catalysts, the doped and the undoped one, showed a shift to lower wavenumbers of the Pt⁰-C stretching band after flushing the systems with Ar. According to Hammaker et al. [53], this band shifted towards lower frequencies as the surface coverage was decreased. Finally, the temperature increase resulted in a progressive decrease of Pt⁰-C band which vanished at about 373 K on Pt/TiO₂ whereas, in the case of Pt/N-TiO₂, at 523 K a low intensity Pt⁰-C band was still observed indicating that CO adsorption is much stronger on the N-doped catalyst.

Pt/TiO₂ and Pt/N-TiO₂ were exposed to a 1% CO/N₂ mixture in order to verify if CO could be oxidized to CO₂ by O atoms of the supports. The evolution of CO conversion as a function of time is shown in Fig. 11. Our results indicate that CO oxidation by O atoms of N-doped and undoped TiO₂ surface is possible but the way in which it occurs is different depending on the catalyst. On Pt/TiO₂, CO conversion decayed with time; however, on the N-doped catalyst, a maximum was observed after 40 min of contact between the sample and the gaseous stream. According to DRIFTS results, CO adsorption is stronger on Pt when the metallic sites are sup-

ported on N-TiO₂, this could explain its lower initial CO conversion compared to Pt/TiO₂.

4. Discussion

The experimental results (Section 3.2) are consistent with the theoretical ones (Section 3.1) in the following items:

- In relation to the electronic structure of the support, the presence of N as a dopant produces a BG narrowing. This was confirmed by the calculated values from DRS spectrum (3.28 eV vs 3.02 eV) and the DOS curves (3.21 eV vs 2.87 eV).
- The DRIFTS spectra of CO adsorbed, after purging with Ar at increasing temperatures (Figs. 9 and 10) show that the characteristic band of the Pt⁰-C bond (between 2085 and 2040 cm^{-1}) disappears at T > 473 K in the N-doped sample, while for the undoped system the temperature drops to 373 K. The CO adsorption energies values and the calculated CO vibration frequencies reinforce this conclusion (Table 4).
- We use the theoretical results (Table 4) to explain the behaviour of the doped system in the CO conversion curve (X_{CO}) vs time (Fig. 11). The initial activity of the undoped system is higher than the doped one, possibly, on one hand, due to its lower CO adsorption energy and, on the other, because of the C charge that is comparatively favorable for subsequent oxidation (1.566e vs 1.638e). After about 10 min from the reaction started, the activity is higher for the doped system presenting a maximum around 40 min; during this period the formation of vacancies is increased and stabilized by the presence of N; from that point, activity starts decreasing being similar to that of the undoped sample after one hour. The analysis of the table shows that the C charge in the doped and reduced system becomes more positive (1.659e) decreasing its capacity to oxidize.
- In summary, research evidence suggests that: (1) the CO is strongly adsorbed on Pt/N-doped surface, (2) the presence of N as dopant favors the oxygen vacancies formation, (3) when the Pt/N-doped surface is reduced, the CO adsorption energy decreases, the Pt-C-O geometry facilitates the reaction between CO and one O surface to form CO₂.

5. Conclusions

In the present study we have examined the geometrical, magnetic and electronic properties of Pt supported on TiO₂(101) (undoped, reduced and/or N-doped) and we have been able to identify the role played by N-doping and oxygen vacancies in the systems analyzed.

Finally, from the analysis of the theoretical and experimental results associated with the CO adsorption energies and the charges and geometry of the atoms involved, it can be concluded that the CO oxidation to CO₂ by oxygen atoms of support surface, is enhanced in Pt/N-TiO₂. In consequence, Pt/N-TiO₂ should favor catalytic reactions in which CO conversion into CO₂ takes place mediated by support surface O atoms.

Acknowledgments

The authors thank the financial support from the Consejo Nacional de Investigaciones Científicas y Técnicas (CONICET) (PIP: 02286), the Universidad Nacional del Sur (UNS) (PGI: 24/F055), the Universidad Nacional del Litoral (UNL) and Agencia Nacional de Promoción Científica y Tecnológica (ANPCyT), Argentina.

References

- [1] S. Ammal, A. Heyden, *J. Catal.* 306 (2013) 78–90.
- [2] D. Andreeva, V. Idakiev, T. Tabakova, L. Ilieva, P. Falaras, A. Bourlinos, *Catal. Today* 72 (2002) 51–57.
- [3] Q. Fu, W. Deng, H. Saltsburg, M. Flytzani-Stephanopoulos, *Appl. Catal. B Environ.* 56 (2005) 57–68.
- [4] X. Wang, R. Gorte, *Appl. Catal. A Gen.* 247 (2003) 157–162.
- [5] R.J. Gorte, S. Zhao, *Catal. Today* 104 (2005) 18–24.
- [6] Y. Bi, H. Xu, W. Li, A. Goldbach, *Int. J. Hydrogen Energy* 34 (2009) 2965–2971.
- [7] G. Jacobs, L. Williams, U. Graham, G.A. Thomas, D.E. Sparks, B.H. Davis, *Appl. Catal. A Gen.* 252 (2003) 107–118.
- [8] F.C. Meunier, A. Goguet, C. Hardacre, R. Burch, D. Thompson, *J. Catal.* 252 (2007) 18–22.
- [9] C. Vignatti, M. Avila, C. Apesteguía, T. Garetto, *Int. J. Hydrogen Energy* 35 (2010) 7302–7312.
- [10] C. Kalamaras, P. Panagiotopoulou, D. Kondarides, A. Efstatithiou, *J. Catal.* 264 (2009) 117–129.
- [11] H. Häkkinen, S. Abbet, A. Sanchez, U. Heiz, U. Landman, *Angew. Chem. Int. Ed.* 42 (2003) 1297–1300.
- [12] H. Liu, H. Ma, X. Li, W. Li, M. Wu, X. Bao, *Chemosphere* 50 (2003) 39–46.
- [13] A. Sirisuk, E. Klansorn, P. Praserthdam, *Catal. Commun.* 9 (2008) 1810–1814.
- [14] N. Sakai, R. Wang, A. Fujishima, T. Watanabe, K. Hashimoto, *J. Phys. Chem. B* 107 (2003) 1028–1035.
- [15] C. Di Valentin, G. Pacchioni, A. Selloni, S. Livraghi, E. Giamello, *J. Phys. Chem. B* 109 (2005) 11414–11419.
- [16] N. Lopez, J.K. Nørskov, *Surf. Sci.* 515 (Issue 1) (2002) 175–186.
- [17] Z. Yan, S. Chinta, A.A. Mohamed, J.P. Fackler Jr., D.W. Goodman, *Catal. Lett.* 111 (1–2) (2006) 15–18.
- [18] M. Gao, A. Lyalin, T. Taketsugu, *Catalysts* 1 (2011) 18–39.
- [19] Y. Han, C. Liu, Q. Ge, *J. Phys. Chem. B* 110 (2006) 7463–7472.
- [20] X. Gong, A. Selloni, O. Dulub, P. Jacobson, U. Diebold, *J. Am. Chem. Soc.* 130 (2008) 370–381.
- [21] P. Scheiber, M. Fidler, O. Dulub, M. Schimidt, U. Diebold, W. Hou, U. Aschauer, A. Selloni, *Phys. Rev. Lett.* 109 (2012) 136103–136105.
- [22] M.M. Islam, M. Calatayud, G. Pacchioni, *J. Phys. Chem. C* 115 (2011) 6809–6814.
- [23] R. Wanbayor, P. Deák, T. Frauenheim, V. Ruangpornvisuti, *J. Chem. Phys.* 134 (2011) 104701–104706.
- [24] W. Hebenstreit, N. Ruzicka, G.S. Herman, Y. Gao, U. Diebold, *Phys. Rev. B* 62 (2000) R16334–16336.
- [25] G. Kresse, J. Hafner, *Phys. Rev. B* 47 (1993) 558–561.
- [26] G. Kresse, J. Hafner, *Phys. Rev. B* 48 (1993) 13115–13118.
- [27] G. Kresse, J. Hafner, *Phys. Rev. B* 49 (1994) 14251–14269.
- [28] J.P. Perdew, J.A. Chevary, S.H. Vosko, K.A. Jackson, M.R. Pederson, D.J. Singh, C. Fiolhais, *Phys. Rev. B* 46 (1992) 6671–6687.
- [29] J.P. Perdew, J.A. Chevary, S.H. Vosko, K.A. Jackson, M.R. Pederson, D.J. Singh, C. Fiolhais, *Phys. Rev. B* 48 (1993) 4978.
- [30] P. Blochl, *Phys. Rev. B* 50 (1994) 17953–17979.
- [31] G. Kresse, D. Joubert, *Phys. Rev. B* 59 (1999) 1758–1775.
- [32] M. Methfessel, A.T. Paxton, *Phys. Rev. B* 40 (1989) 3616–3621.
- [33] V. Anisimov, J. Zaanen, O. Andersen, *Phys. Rev. B* 44 (1991) 943–954.
- [34] C.I.N. Morgade, G.F. Cabeza, N.J. Castellani, Proceeding XXIII Congreso Iberoamericano de Catálisis, Santa Fe, Argentina, 2012.
- [35] S. Dudarev, G. Botton, S. Savrasov, C. Humphreys, A. Sutton, *Phys. Rev. B* 57 (1998) 1505–1509.
- [36] R.F.W. Bader, *Atoms in Molecules: A Quantum Theory*, Oxford University Press, Oxford, 1990.
- [37] E. Finazzi, C. Di Valentin, A. Selloni, G. Pacchioni, *J. Phys. Chem. C* 111 (2007) 9275–9282.
- [38] J. Wang, W. Zhu, S. Liu, *J. Phys. Chem. C* 111 (2007) 1010–1014.
- [39] J.M. Sinfelt, J.L. Carter, D.J.C. Yates, *J. Catal.* 24 (1972) 283–296.
- [40] T.F. Garetto, C.R. Apesteguía, *Catal. Today* 62 (2000) 189–199.
- [41] Y. Ying, F. Quing, W. Weihua, W. Yin, *J. Semicond.* 34 (2013), 73004–1–5.
- [42] N. Portillo Velez, O. Olivera Neria, I. Hernandez Perez, A. Rubio Ponce, *Surf. Sci.* 616 (2013) 115–119.
- [43] K. Yang, Y. Dai, B. Huang, Y. Ping Feng, *Phys. Rev. B* 81 (2010) 33202–33204.
- [44] M. Batzill, E. Morales, U. Diebold, *Phys. Rev. Lett.* 96 (2006), 26103–1–4.
- [45] J. Tauc, R. Grigorovici, A. Vancu, *Phys. Status Solidi* 15 (1966) 627–637.
- [46] F. Abeles, in: F. Abeles (Ed.), *Optical properties of solids*, North-Holland Pub. Co.; American Elsevier Amsterdam, New York, 1972.
- [47] Q. Chen, Ch. Tang, G. Zheng, *Phys. B* 404 (2009) 1074–1078.
- [48] G. Blyholder, *J. Phys. Chem.* 68 (1964) 2772–2778.
- [49] K. Momma, F. Izumi, *J. Appl. Crystallogr.* 44 (2011) 1272–1276.
- [50] P.T. Fanson, W.N. Delgass, J. Lauterbach, *J. Catal.* 204 (2001) 35–52.
- [51] N. Sheppard, T.T. Nguyen, in: R.J.H. Clark, R.E. Hester (Eds.), *Advances in Infrared and Raman Spectroscopy*, Vol. 5, Heyden, London, 1978, p. 67.
- [52] P. Panagiotopoulou, A. Christodoulakis, D. Kondarides, S. Boghosian, *J. Catal.* 240 (2006) 114–125.
- [53] R. Hammaker, S. Francis, R. Eischens, *Spectrochim. Acta* 21 (1965) 1295–1309.